Turkish Journal of Electrical Engineering & Computer Sciences

http://journals.tubitak.gov.tr/elektrik/

Research Article

Turk J Elec Eng & Comp Sci
(2020) 28: 2702 – 2717

doi:10.3906/elk-2001-107

Formation of a wireless sensor network using custom-designed sensors having low power and low cost components

Veysel Yaman AKGÜN[1], **Engin MAŞAZADE**[2,*]

[1]Department of Electrical and Electronics Engineering, Faculty of Engineering, Yeditepe University, İstanbul, Turkey

[2]Department of Electrical and Electronics Engineering, Faculty of Engineering, Marmara University, İstanbul, Turkey

Received: 23.01.2020 • **Accepted/Published Online:** 04.05.2020 • **Final Version:** 25.09.2020

Abstract: In this paper, we first design a sensor with low power and low cost components, namely an MSP430G2553 microcontroller (MCU), nRF24L01+ communication unit, and a light-dependent resistor (LDR). Then, connecting these custom-designed sensors with a central node, a fusion center (FC), we form a wireless sensor network (WSN) in which sensors measure light intensities and send their measurements to the FC for final inference. Since the default addressing structure of nRF24L01+ can simultaneously connect up to 6 devices, in order to have more connections, we define a new addressing scheme for the transmissions between sensors and the FC. Finally, as a test case, we consider the task of the WSN in field estimation. The FC learns the spatial dependence between sensor measurements called a variogram. Then, using the appropriate variogram model, we perform ordinary kriging (OK), where the light intensity at an unobserved location is estimated as a weighted sum of received LDR measurements. Our test results show that the estimated light measurement using OK at a specific location becomes quite close to the actual LDR measurement at that location under the suitable parametric variogram models.

Key words: Node design, medium access control, wireless sensor networks, field estimation

1. Introduction

Wireless sensor networks (WSNs) observe the relevant quantities of a certain region using a number of sensors. Then sensor measurements are gathered at a fusion center (FC), which makes a statistical inference. Since sensors are considered simple, cheap, battery-powered devices [1], the sensors, and hence the WSN, need to be both energy efficient and low cost in order to maximize the lifetime of the network and minimize the deployment costs.

It is possible to develop various WSN applications using commercially available sensors such as MICAz, Telos, iMote2, and Xbee [2–4]. When a WSN is formed by using such commercial nodes, the programming burden required for the wireless communications, medium access control operations, and the internal sensor operations are significantly lifted from the network designer, and the designer can more focus on the application and inference results. On the other hand, forming a WSN with such commercial nodes may create a serious cost for a limited budget study. As an example, the price of a single TelosB module is typically around 90 Euros[1].

*Correspondence: engin.masazade@marmara.edu.tr

[1]ADVANTICSYS (2020). 802.15.4 Mote Modules [online]. Website: https://www.advanticsys.com [accessed 20 January 2020].

Fortunately, it is also possible to create a sensor node with low cost and low energy consumption by carefully choosing its fundamental elements such as its microcontroller unit (MCU), communication unit, and sensing unit [5]. Texas Instruments (TI) MSP430 family MCUs are used popularly in commercially available sensors due to their low power consumption and low cost. As an example, the TelosB module uses TI MSP430F2618 as its MCU. As compared to MSP430F series, MSP430G series MCUs are simpler and cheaper and provide ultra-low power consumption. In the literature, MSP430G series MCUs appear as the MCU of a wireless node in limited designs. As an example, for a unidirectional communication [6] or a bidirectional communication [7] both the transmitter and the receiver employ an MSP430G2553 MCU.

There are various alternatives for the wireless transceiver module to be connected to the MCU. These transceivers commonly operate at the license-free 2.4 GHz Industrial, Scientific and Medical (ISM) radio bands. TI-based CC1101, CC24XX, CC25XX, or similar wireless modules can be easily embedded in MSP430 MCUs to design a sensor. On the other hand, Nordic Semiconductor's nRF24L01 wireless module provides lower cost and lower power consumption as compared to CC1101 and Wi-Fi modules [8], CC24XX [9, 10], and CC25XX [10]. For a sensor node design, a nRF24L01 wireless module was used together with Atmel ARM based MCUs [11–16]. Thanks to their ultra-low power consumption, nRF24L01+ transceivers have also been used with MSP430F series MCUs where to best of our knowledge there is no proof of concept WSN application in the literature, whose sensors are formed with low cost, simple, ultra-low power MSP430G2553 series MCU, and the nRF24L01+ wireless transceiver. When nRF24L01 is used with MSP430F series MCUs, studies typically consider a transmission between a simple transmitter and a receiver pair [11, 12, 15–17]. The default addressing structure of nRF24L01+ enables simultaneous connections of up to six transmitters to a particular receiver[2]. Therefore, by using the default addressing scheme, previous works [13, 18] consider a limited number of nodes transmitting to a central receiving node. In order to connect more than 6 nodes to a central node, in Ma and Pan [14], a central node sequentially visits each node in the WSN. Furthermore, in Christ et al. [19] various transmitters and receivers employing nRF24L01 have been deployed and the trade-offs between data rate and package length versus the number of lost packets have been observed under different operating frequencies, packet sizes, and numbers of transmitters.

Different sensing modalities can be embedded in the sensor node design. Temperature, humidity, light intensity, and similar sensors can be used for environmental monitoring applications [3, 14–16]. A light-dependent resistor (LDR) can be included in the wireless sensor node design in order to measure the light intensity in a given region of interest. In the present work we choose LDRs, since it is easy to calibrate different LDRs under a given lighting condition and it is also easy to form a test region for the WSN under different lighting conditions.

Upon completing the design of a wireless sensor node and forming a WSN with such custom-designed sensors, the collected sensor measurements at the FC can be transferred to a computationally powerful personal computer (PC). As a use case here, we consider the task as field estimation. In field estimation, based on the received sensor measurements observed from known sensor locations, the field intensity at an unobserved location is predicted [20, 21]. Field estimation using WSNs has been used in many application areas, such as in precision agriculture to monitor soil moisture [22], or in weather activity monitoring such as weather temperature prediction [21]. For field estimation, based on the received sensor measurements observed at known locations, the spatial relation between the measurements, which is quantified by the spatial variogram, needs to be first

[2]NORDIC Semiconductor (2020). nRF24L01+ Single Chip 2.4GHz Transceiver Product Specification v1.0 [online]. Website: https://www.nordicsemi.com [accessed 20 January 2020].

estimated. Upon having the variogram model, field estimation can then be performed by using ordinary kriging (OK) [20, 21].

The key contribution of our work originates from custom sensor and hence WSN design, and experimental measurements of such sensors for statistical inference. Custom-designed sensors with similar components were either considered for transmission between a simple transmitter and receiver pair [11, 12, 15–17], or using such sensors a small-size WSN was formed with a small number of nodes due to the default addressing scheme of nRF24L01+ [13, 14, 18]. In the present work, in order to connect more sensors, we first modify the default addressing scheme of nRF24L01+, where the fusion center is able to gather sensor measurements from more than 6 nodes and able to send all of the gathered sensor measurements to a powerful computer for further statistical inference as field estimation. Using commercial MICAz motes, there exist serious WSN realizations for field estimation [3, 4]. However, in the present work, we propose a proof-of-concept system where rather than using relatively costly commercial nodes we perform field estimation using custom-designed sensors composed of low cost and low energy components. Note that we presented a preliminary version of this study previously [23]. As compared to that study [23], herein we comprehensively present the sensor node design and addressing procedures. Furthermore, previously [23] we tested the proposed WSN for field estimation under the linear variogram model only. In the present article, we compare field estimation performance under 5 different variogram models where Gaussian and Matérn variogram models fit better to the lighting conditions in a classroom environment rather than the bounded linear, spherical, and exponential models.

The rest of the article is organized as follows: In Section 2, we explain the sensor design. In Section 3, we present the MAC protocol and the addressing schemes. In Section 4, we briefly explain the mathematical foundations of the field estimation problem. In Section 5, we present our test results and finally we devote Section 6 to our conclusions and address potential research directions.

2. Design of a sensor node

In this section, we examine the fundamental components of the proposed sensor node as presented in Figure 1a in detail.

2.1. Microcontroller

MSP430G series MCUs are simpler and cheaper and provide low power consumption as compared to MSP430F series MCUs. Here we can compare the technical specifications of MSP430G2553 and MSP430F2613, which used in a TelosB node. MSP430G2553 is simpler than MSP430F2618 since it has fewer I/O's, less RAM, less memory size, fewer communication interfaces, and less ADC resolution. On the other hand, the limited capabilities of MSP430G2553 are still sufficient to perform the simple operations, and the price of a single MSP430G2553 MCU is around 2.65 USD whereas the price of a MSP430F2618 MCU is around 12 USD [3]. Therefore, due to its simplicity, low cost, and low energy consumption, in the present paper we select MSP430G2553 as the MCU of the sensor node.

MSP430G2553 has a central processing unit (CPU) with operating frequency up to 16 MHz [4]. It supports communication protocols to connect to other MCUs and peripheral devices using an inter-integrated circuit (I^2C), serial peripheral interface (SPI), and universal asynchronous receiver/transmitter (UART). Note that

[3]Mouser Electronics (2020). Texas Instruments MSP430F2618TZQWR [online]. Website: http://www2.mouser.com/ [accessed 20 January 2020]

[4]Texas Instruments (TI) MSP430G2x53 (2020), MSP430G2x13 Mixed Signal Microcontroller (Rev. J). [online] http://www.ti.com/lit/gpn/msp430g2553 [accessed 20 January 2020].

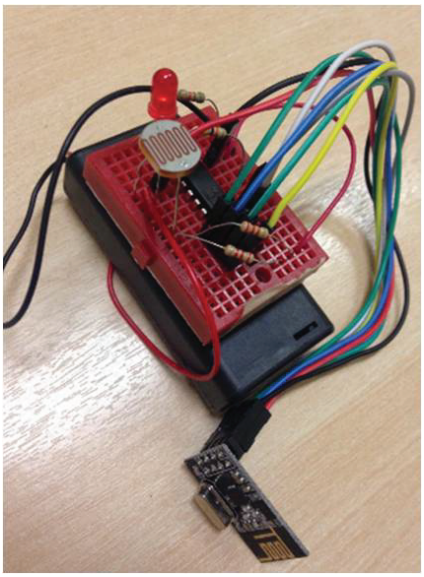

(a)

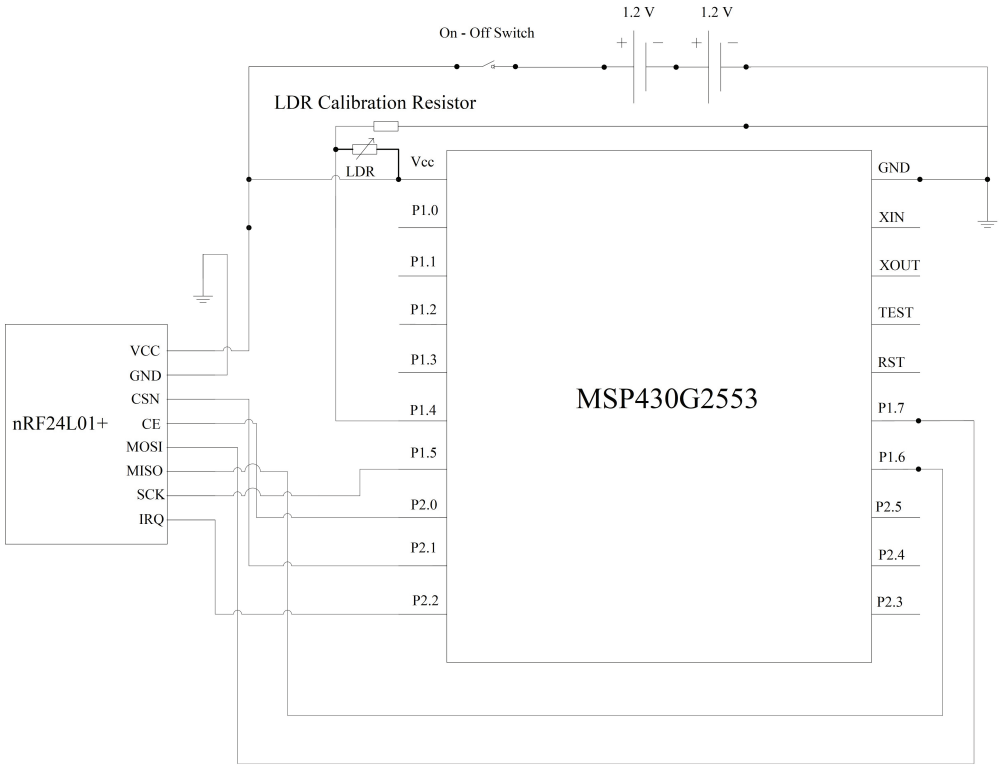

(b)

Figure 1. (a) A view of a designed sensor node, (b) circuit schematic of sensor node.

in the present work the communication between nRF24L01+ and MCU requires an SPI. Since the maximum clock cycle limit for communication via SPI between MSP430G2553 and nRF24L01+ is limited to 8 MHz, the

operating frequency of MSP430G2553 is set to 8 MHz. Moreover, MSP430G2553 has 8 analogue to digital converter (ADC) channels. Note that the ADC operations are done in 10 bits.

In addition, the circuit schematic between MSP430G2553 and nRF24L01+ is shown in Figure 1b. nRF24L01+ has 8 pins, which are ground (GND), IC power-supply pin (VCC), chip enable (CE) for RX/TX enable, chip select not (CSN) for enabling SPI commands & responds, SPI shift clock (SCK) for SPI clock up to 10 MHz, master-out-slave-in (MOSI) for SPI output to send data from MCU to nRF24L01+, master-in-slave-out (MISO) for SPI input to send data from nRF24L01+ to MCU, and optional interrupt request (IRQ) for interrupts about receive (RX) or transmit (TX) status in the case of a received or a sent packet. Briefly, CE, CSN, SCK, and MOSI are inputs and MISO and IRQ are outputs of nRF24L01+. In Figure 1b, P 1.1 and P 1.2 of MSP430G2553 are reserved for UART operations. Moreover, the ADC measurement is obtained by using P 1.4. P 1.5 is used as SPI CLK, P 1.6 is used as SPI MISO, and P 1.7 is used as SPI as MOSI in the 3-pin SPI. Furthermore, P 2.0, P 2.1, and P 2.2 are used for CE, CSN, and IRQ, respectively. Additionally, the system is supplied with two 1.2 V AA rechargeable batteries and there is an on/off switch to turn on or shutdown the node completely.

2.2. Transceiver unit

The nRF24L01+ single chip transceiver antenna operates at the 2.4 GHz ISM band. It supports 126 channels from 2.4 GHz to 2.525 GHz. The data rates can be selected as 250 kbps, 1 Mbps, or 2 Mbps. The nRF24L01+ channel spacing is 1 MHz, which gives 126 possible channels for 250 kbps and 1 Mbps data rates, and the channel spacing is 2 MHz for a 2 Mbps air data rate. nRF24L01+ uses Gaussian frequency shift keying (GFSK) modulation at the radio front end. The price of the nRF24L01+ is around 1 USD [5]. The chip of nRF24L01+ operates at ultra-low power as in the MCU. It consumes about 11.3 mA while transmitting a data packet at 0 dBm output power level, and it consumes about 13.5 mA while receiving at 2 Mbps air data rate. Furthermore, it consumes 900 nA in power-down mode and 26 μA in the standby mode called standby-I. Moreover, there is a voltage regulator on the chip and the supply range is so wide from 1.9 V to 3.6 V to be sufficient for common feeding levels. In the present work, we select the output power of nRF24L01+ as 0 dbM. In addition, the data rate is selected as 1 Mbps at the 121st channel operating at 2.520 GHz.

In receiver mode, nRF24L01+ has six parallel data pipes that enable simultaneous connections with up to six transmitters at a certain frequency channel. Each pipe is represented by a unique address, and nRF24L01+ sequentially checks the content in each data pipe address. The receiver (PRX) can utilize six different pipe addresses to receive data from six associated transmitters (PTX). All data pipes can operate with the Enhanced ShockBurst^{TM} packet format. The first part of the packet is used to synchronize with the receiver. The second part is the receiver address, which includes the pipe address of the receiving nRF24L01+ unit. The third part is the packet control field. It is composed of 9 bits. The fourth section of the payload can be defined by the user. The payload size can be selected up to 32 bytes. In the present work, we select a fixed payload size for the transmissions from each sensor to FC and FC to sensors as 16 bytes. We form the payload with the receiver no id, the transmitter no id, and the measurement. Finally, the last part of the packet is the cyclic redundancy check (CRC), which is responsible for error detection mechanism. There are also three acknowledgment (ACK) options in the nRF24L01+ unit, which are no ACK, ACK with empty package, and ACK with payload. For the present study, we select ACK with payload, where the ACK packet contains an exact copy of the received payload.

[5] Amazon (2020). Makerfire 10pcs Arduino nRF24L01+ 2.4GHz Wireless RF Transceiver Module New. Website: https://www.amazon.com [accessed 20 January 2020.

Since each payload has specific and unique information like sensor node number, basic timing information, and measurements, the transmitter validates the received ACK with its previously transmitted payload.

2.3. Sensing unit (LDR)

The LDR and its calibration resistor are connected in series as shown in Figure 1b. The LDR is connected to one of the 8 ADC pins of the MCU. As seen in Figure 1b, pin 1.4 of the MCU is used in this work. Along with the LDR, temperature and voltage values are also obtained in 10 bit resolution using an ADC. Since each payload byte of the nRF24L01+ has 8 bits, in the present work, we quantize 10 bit ADC measurements into 8 bits by removing the least significant 2 bits of the ADC values. The average value of the 20 LDR measurements read from the ADC is taken as the final measurement to prevent instantaneous measurement errors and minimize the effect of outlier measurements.

Note that a calibration procedure is necessary in order to observe reliable measurements under the same lighting condition. For calibration, we form the circuit shown in Figure 2a. Firstly, an LDR is placed with a potentiometer connected in series under a given amount of light intensity to determine the reference voltage output. The supply voltage level (Vcc) is adjusted to 2.8 V. At a certain light intensity, the reference output level (Vout) is adjusted to 1.5 V by spinning the potentiometer adjustment stick. When the desired output is reached, the potentiometer resistance is noted, which represents the ideal value of the calibration resistor. Finally, we select the closest resistor in practice to the ideal calibration resistor value. The closest resistor can be obtained as a combination of two or more resistors connected in series or parallel. Next we obtain the relationship between the input and the output voltages of the LDR (Vin and Vout). Vcc is set to 2.8 V and then a 1 W light emitting diode (LED) light source is located at the same axis and direction as the LDR where the LED light source and the LDR face each other. The distance between the LDR and LED is set to 10 cm. The voltage of the LED (Vin) is increased from 2 V to 4.5 V gradually. While the input voltage of the LED increases, the brightness of the LED also increases. The relationships between input and output voltages of the 11 LDRs used in the present work after calibration are shown in Figure 2b. In our work, under the relevant test area conditions, we observe that the output LDR voltages (Vout) vary between 0 V and 1.6 V. Therefore, sensory device characteristics become similar to each other at the operating range.

2.4. Current consumption and cost of components

We show the current consumption of each component in Table 1. We determine the current consumption of the components under 2.75 V supply. In active mode, MSP430G2553 drains around 230 μA. In receiving mode, nRF24L01+ drains around 14 mA. LDR drains around 0.15 mA to 2 mA depending on the light intensity of the medium. Under low and bright lighting conditions, the proposed sensor device drains around 14.6 mA and 16.4 mA, respectively. Under high light conditions, with 2500 mAh batteries, the overall system may last actively around 152 h. Furthermore, the price of each component is roughly shown in Table 2. As of market prices in January 2020, a sensor node costs around 12 USD.

3. MAC protocol of the WSN

In this section, we present the MAC protocol and the addressing structure used to connect sensors with the FC. The FC further forwards the sensor measurements to a PC. Here the FC is directly connected to a PC, and it consists of MSP430G2553 and nRF24L01+. There is a duplex communication via wire between FC and PC using the COM port interface. There is a hardware UART converter at the MSP430G2553 LaunchPad. Then

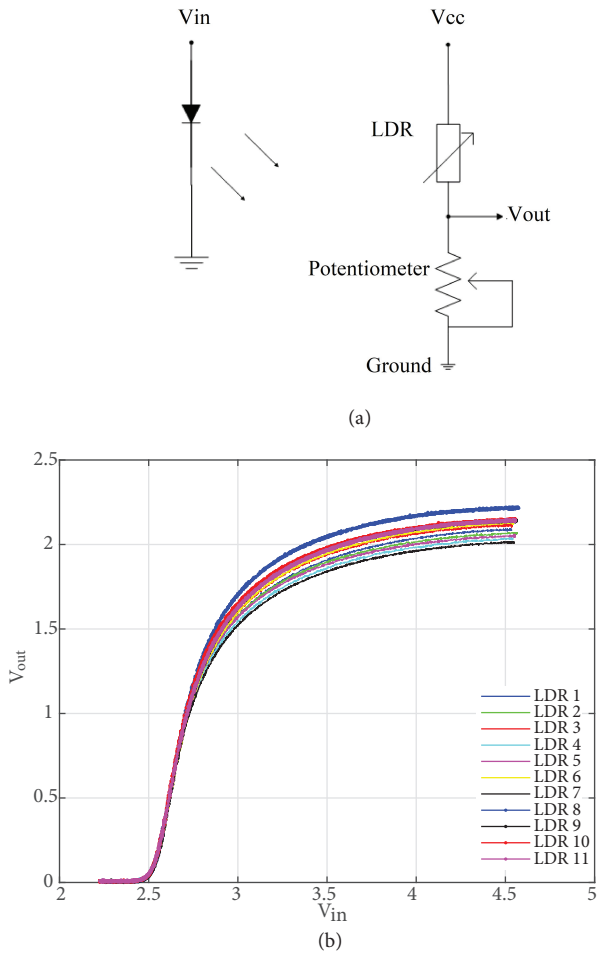

Figure 2. (a) Calibration circuit diagram, (b) characteristics of the LDRs.

Table 1. Current consumption of each component at the sensor node.

	Components				
	MSP430G2553	nRF24L01+	LDR	Overall system	
Description	Active Mode(AM)			Under Low Light	Under High Light
Current consumption @2.75V	230μA	~14mA	0,15mA~2mA	**14,6 mA**	**16,4 mA**

the FC MCU communicates with the PC by using its UART protocol, and communicates with the nRF24L01+ via its SPI protocol. The data sent from the FC by using UART are converted to serial port (COM port) data on the PC. Then computer-based software executes the field estimation, which will be explained in Section 4 in detail.

In our system, gathering of sensor measurements is initialized by the user on the PC. When the FC receives a request from the PC, the FC makes a data request to all sensors by using a broadcast message and

Table 2. Cost of each component.

Item	Description	Price (in $)
1	MSP430G2553	2.8
2	nRF24L01+	0.99
3	Sensor (LDR)	0.35
4	Batteries (2 x AA 2500 mAh)	4.75
5	Mini breadboard	0.71
6	Other components (Cable, resistor, battery box, etc.)	2
	General Total	**11.60 $**

waits for the individual sensor replies. When the FC receives a sensor measurement, it sends an ACK back to that sensor. When the FC receives all the sensor data or after the timeout period expires, it sends the collected sensor data to the PC. Then the FC clears the sensor data on its registers to enable another request from the PC.

By using only 6 pipes assigned to each sensor as described in Section 2.2, we are unable to implement a FC that simultaneously receives measurements from more than 6 sensors at a given frequency channel. Therefore, in order to connect more sensors to the FC, we use only two of the pipes. Pipe 0 addresses of each sensor and the FC is used for data transmissions between sensors and the FC, and pipe 1 addresses of sensors and the FC are used for initial data requests from FC to sensors. In Figure 3, we show $N = 11$ sensors and the FC where the initial pipe 0, pipe 1, and transmit addresses are defined. Note that pipe 0 addresses of sensors and the FC are set uniquely, while pipe 1 addresses of sensors and the FC are selected the same. As an example, when the FC transmits a data request packet, the receive address segment in the packet format is filled with the common pipe 1 address 0xDEADBEEFC8. When a sensor receives this data request, it compares the packet address with its own pipe 1 addresses. Since the addresses match each other, the sensor obtains the measurement and prepares its data packet payload. In other words, a sensor listens to the medium until it receives a request from its pipe 1. The data packet is sent to the pipe 0 address of the FC.

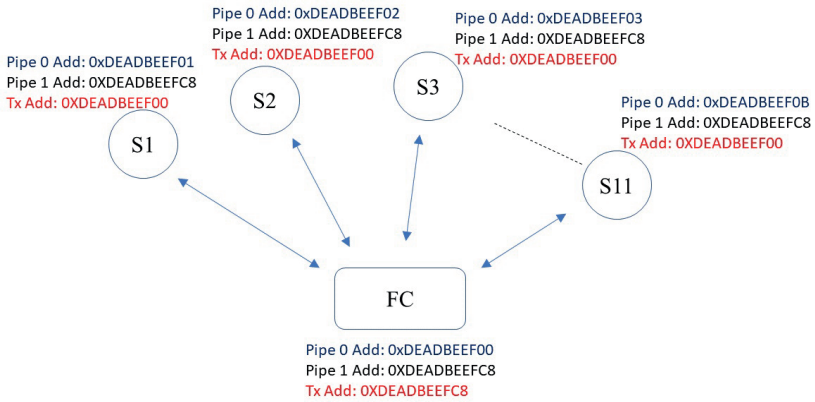

Figure 3. Addressing scheme at each sensor and the FC.

Before transmitting to the FC, sensors first check the activity in the medium. If the medium is idle, they transmit. A received power detector (RPD) is used to conclude on the channel activity. If nRF24L01+ detects activity, for the worst case scenario, it waits for two maximum packet duration, where the packet duration is computed based on the packet format with a full payload size of 32 bytes. At the end of this period, the sensor checks the medium again, and if there is no channel activity, it sends its packet. Otherwise, it keeps waiting for another two maximum packet duration.

For data reply, in our setting, pipe 0 addresses of sensors and the FC are selected uniquely. Therefore, upon transmitting the data packet to the FC, a sensor should immediately turn its pipe 0 address into the pipe 0 address of the FC. As an example, in Figure 3, sensor 1 has an initial pipe 0 address of 0xDEADBEEF01. Upon transmitting its data packet to the FC, it must update its pipe 0 address to the pipe 0 address of the FC, i.e. 0xDEADBEEF00. By doing so, now sensor 1 becomes ready to capture the ACK corresponding to its transmission. Since the rest of the sensors will have different pipe 0 addresses at that instant, the ACK of sensor 1's transmission may be received only by sensor 1. Upon reception of the ACK, the sensor updates its pipe 0 address to its initial value and waits for another data request from the FC. As in the example, upon receiving the ACK, sensor 1 sets its pipe 0 address back to 0xDEADBEEF01.

It is also possible that two or more sensors send their packet to the pipe 0 address of the FC at the same time. In this case, both sensors change their pipe 0 address to the pipe 0 address of the FC and wait for ACK. If there is a collision, none of them receive any ACKs and they should retransmit their packets. On the other hand, when the FC receives one of the data packets from its pipe 0, it will send an ACK with the entire contents of the received payload data. In this case, sensors receiving this ACK compare the ACK content with the previously transmitted payload content. Then only the sensor whose transmitted payload matches the content of the received ACK concludes that its transmission was successful. The other sensors whose transmitted payload data do not match the ACK payload understand a failure and perform retransmission.

Upon transmission of the packet to the FC, the nRF24L01+ of the sensor waits 4000 μs for reception of the associated ACK. If no ACK is received within this period, the packet is automatically retransmitted. In the present work, each data packet from sensors to FC is transmitted automatically at most 10 times. After the completion of the 10th transmission, if the sensor still has not yet received an ACK from the FC, it concludes a transmission failure. Failures may occur as a result of the packet collisions that occur as a result of simultaneous transmissions. If a sensor realizes a transmission failure, it first waits for some duration proportional to its node ID. This aims to prevent simultaneous transmissions of the previously failed packets. As an example, in our WSN, sensor 1 waits less time and sensor 11 waits more time before retransmitting its packet. At the end of this period, each sensor updates its packet content with new measurements from the LDR and then checks the medium. If the medium is clear, the sensor transmits its packet to the FC. If the medium is busy, the sensor waits for two maximum packet durations as described above.

At the FC, nRF24L01+ receives data when the incoming packet address matches its pipe 0 addresses. Then nRF24L01+ notifies the MCU of this situation. Next the MCU checks the sensor id located inside the payload and stores the measurement received from that sensor. It is also possible that the FC may receive the data packet of a particular sensor but the associated ACK might not be received by the sensor. In this case, the sensor concludes a transmission failure and execute the process described above. If the FC receives multiple packets from the same sensor, it overwrites the packets received from this sensor. In other words, the last successfully received packet coming from the sensor is stored in the FC's respective register. Finally, when a sensor receives the ACK of its transmitted packet, it restarts its hardware by using the watchdog timer (WDT).

Afterwards, the sensor goes into listening mode and keeps checking its pipe 1 to detect another request from the FC.

4. Field estimation

We forward all the sensor measurements gathered at the FC MCU to a PC for statistical inference, where we consider field estimation [20, 21]. Other applications such as target detection or target localization can be also performed in a similar fashion. In this section, we follow the notation presented in Lichtenstern [21].

4.1. Variogram

The variogram measures the spatial relation of the random process $z(\mathbf{x})$ over the field of interest. In other words, it measures how two different measurements, $z(\mathbf{x}_i)$ and $z(\mathbf{x}_j)$ observed at locations $\mathbf{x}_i$ and $\mathbf{x}_j$, influence each other. The variogram can be estimated from a sample of data collected from certain locations of the field. Let a pair of sensor measurements obtained from the field be represented by $z(\mathbf{x}_i), \ldots, z(\mathbf{x}_j)$. Then the experimental variogram yields a measure of dependence as

$$\gamma^*(\mathbf{h}) = \frac{1}{2N(\mathbf{h})} \sum_{N(\mathbf{h})} (z(\mathbf{x}_i) - z(\mathbf{x}_j))^2 \tag{1}$$

Here $N(\mathbf{h})$ represents the number of sensor pairs whose distances are $\mathbf{h}$, i.e. $N(\mathbf{h}) = \{\mathbf{h} = \mathbf{x}_i - \mathbf{x}_j, i, j \in 1, \ldots, N\}$. We next use the parametric variogram models for curve fitting to the experimental variogram [21]. For the parametric variogram models, i.e. bounded linear, spherical, exponential, Gaussian, or Matérn, $\gamma_{a,b}(\mathbf{h})$ with lag h, $a, b > 0$ represent the model parameters, where a represents the range parameter and b represents the sill value [21] as in

- Bounded linear model:

$$\gamma_{a,b}(\mathbf{h}) = \begin{cases} b\left(\frac{|\mathbf{h}|}{a}\right) & 0 \le |\mathbf{h}| \le a \\ b & elsewhere \end{cases} \tag{2}$$

- Spherical model

$$\gamma_{a,b}(\mathbf{h}) = \begin{cases} b\left[\frac{3}{2}\frac{|\mathbf{h}|}{a} - \frac{1}{2}\left(\frac{|\mathbf{h}|}{a}\right)^3\right] & 0 \le |\mathbf{h}| \le a \\ b & elsewhere \end{cases} \tag{3}$$

- Exponential model

$$\gamma_{a,b}(\mathbf{h}) = b\left[1 - \exp\left(-\frac{|\mathbf{h}|}{a}\right)\right] \quad |\mathbf{h}| \ge 0 \tag{4}$$

- Gaussian model

$$\gamma_{a,b}(\mathbf{h}) = b\left[1 - \exp\left(-\frac{|\mathbf{h}|^2}{a^2}\right)\right] \quad |\mathbf{h}| \ge 0 \tag{5}$$

- Matérn model

$$\gamma_{a,b,v}(\mathbf{h}) = b\left[1 - \frac{1}{2^{v-1}\Gamma(v)}\left(\frac{|\mathbf{h}|}{a}\right)^v I_v\left(\frac{|\mathbf{h}|}{a}\right)\right] \quad |\mathbf{h}| \ge 0\ , \tag{6}$$

where v is the smoothness parameter, $v \in [0, \infty)$, $\Gamma(.)$ is the gamma function, and $I_v(.)$ is the modified Bessel function of order v.

For each parametric variogram model, we fit its parameters a, b (and v for the Matérn model only) by minimizing the error between the experimental variogram $\gamma^*(\mathbf{h})$ and the selected parametric variogram model $\gamma_{a,b}(\mathbf{h})$ as

$$\min_{a,b} \sum_{\mathbf{h}} \left(\gamma^*(\mathbf{h}) - \gamma_{a,b}(\mathbf{h})\right)^2 \tag{7}$$

4.2. Ordinary kriging

In the present paper, we use the OK method in order to estimate the field intensity at an unobserved location using the received sensor measurements [20, 21]. Assume that the field is sampled by N sensors at known locations $\mathbf{x}_i$, where $i \in \{1, 2, \ldots, N\}$. Let each sensor measurement observed at location $\mathbf{x}_i$ be represented as $z(\mathbf{x}_i)$ Then the OK estimate of the field intensity at a certain location $\mathbf{x}_0$, $\hat{z}(\mathbf{x}_0)$, is obtained by taking the linear combination of sensor measurements as

$$\hat{z}(\mathbf{x}_0) = \sum_{i=1}^{N} \lambda_i z(\mathbf{x}_i), \tag{8}$$

where λ_i represents the unknown weights. In order to ensure that the OK estimator is unbiased, i.e. $E[\hat{Z}(\mathbf{x}_0) - Z(\mathbf{x}_0)] = 0$, the sum of weights needs to be set to one $\sum_{i=1}^{N} \lambda_i = 1$. OK then minimizes the estimation error variance $\sigma^2_{\boldsymbol{\lambda}}(\mathbf{x}_0) = E\left[\left(\hat{z}(\mathbf{x}_0) - z(\mathbf{x}_0)\right)^2\right]$ subject to the constraint that $\sum_{i=1}^{N} \lambda_i = 1$. The constraint of the optimization problem can be further added to the objective function as

$$\min_{\lambda_1,\ldots,\lambda_N,\alpha} E\left[\left(\hat{z}(\mathbf{x}_0) - z(\mathbf{x}_0)\right)^2\right] - \alpha\left(\sum_{i=1}^{N} \lambda_i - 1\right), \tag{9}$$

where α represents the Lagrange multiplier. The problem in (9) can be solved using Newton's method and the optimal solution set can be obtained from [21]

$$\begin{bmatrix} \lambda_1^* \\ \vdots \\ \lambda_N^* \\ \alpha^* \end{bmatrix} = \begin{bmatrix} \gamma(\mathbf{x}_1 - \mathbf{x}_1) & \ldots & \gamma(\mathbf{x}_1 - \mathbf{x}_N) & 1 \\ \gamma(\mathbf{x}_2 - \mathbf{x}_1) & \ldots & \gamma(\mathbf{x}_2 - \mathbf{x}_N) & 1 \\ \vdots & \ldots & \vdots & \vdots \\ \gamma(\mathbf{x}_N - \mathbf{x}_1) & \ldots & \gamma(\mathbf{x}_N - \mathbf{x}_N) & 1 \\ 1 & \ldots & 1 & 0 \end{bmatrix}^{-1} \begin{bmatrix} \gamma(\mathbf{x}_1 - \mathbf{x}_0) \\ \vdots \\ \gamma(\mathbf{x}_N - \mathbf{x}_0) \\ 1 \end{bmatrix}$$

Here $\boldsymbol{\lambda}^* = [\lambda_1^*, \ldots, \lambda_N^*]^T$ represents the vector yielding the optimal OK weights, and α^* is the Lagrange multiplier of OK. Upon computing the optimal OK weights and the Lagrange multiplier, the estimation error variance can be computed as [21]

$$\sigma^2_{\boldsymbol{\lambda}}(\mathbf{x}_0) = \alpha^* + \sum_{i=1}^{N} \lambda_i^* \gamma(\mathbf{x}_i - \mathbf{x}_0) \tag{10}$$

5. Test results

In this section, we present the test results obtained from the field using the developed wireless sensor network. As described in Section 2, we form 11 sensors and the FC. The MCUs are programmed in C using TI's Code

Composer Studio where the functions and the headers of nRF24L01+ are publicly available[6]. The sensors and the FC are deployed inside the test area as shown in Figure 4a. We use the Simulation Laboratory of Yeditepe University as the test area as shown in Figure 4b. Note that the lights corresponding to the top left and bottom right in Figure 4a of the laboratory are turned on during our experiments. The computer-based software we use is MATLAB.

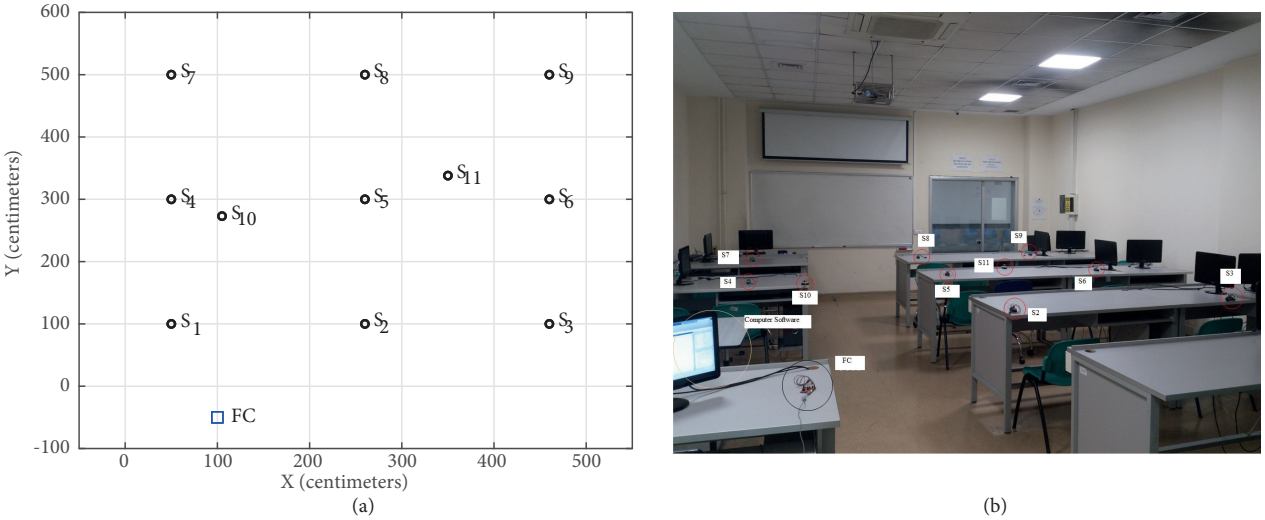

Figure 4. (a) Deployment of sensors and the FC inside the test area, (b) a view of the test area from the FC location.

We first perform 500 trials, namely data gathering from the WSN, and in Figure 5a we show the histogram of the total elapsed time from the beginning of the data request from the FC until the reception of all $N = 11$ sensor measurements. Our test results show that in around 60% of trials the entire WSN data are collected at the FC in less than 4 s. Note that we set the time-out duration as 20 s, and we can observe in the figure that the total number of trials in the histogram adds up to around 500 with few trials where $N = 11$ sensor measurements cannot be gathered.

We next obtain the experimental variogram as defined in (1). Then we find the optimized parameters of the bounded linear, spherical, exponential, Gaussian, or Matérn variogram model fitting to the experimental variogram. For the optimization problem in (7), we determine the optimal values of the variogram model parameters (a, b, and v) by using MATLAB's fmincon function with its default settings. Figure 5b shows the variogram models fitted to the experimental variogram. For the sensor deployment in Figure 4a, we have a relatively large number of inter-sensor distances below 3 m and a smaller number of distances above 3 m. Due to the averaging in (1), the mathematical variogram models fit well to the experimental variogram for shorter distances, whereas for longer distances we observe outliers. The effect of such outlier dissimilarity values may be reduced in the future by having more samples at such distances.

Table 3 shows the optimized variogram model parameters for the expressions in (2) to (6), estimated measurements, and the relative error between the estimated measurement and the actual sensor measurement at that location. From Figure 4a, we use S5, S10, or S11 as a test sensor whose measurement is estimated using the measurements of rest of the other 10 sensors. Since S5, S10, and S11 are located relatively in the center of

[6]GitHub (2020). nRF24L01+ Library for MSP430 Microcontroller Line [online]. Website: https://github.com/spirilis/msprf24 [accessed 20 January 2020].

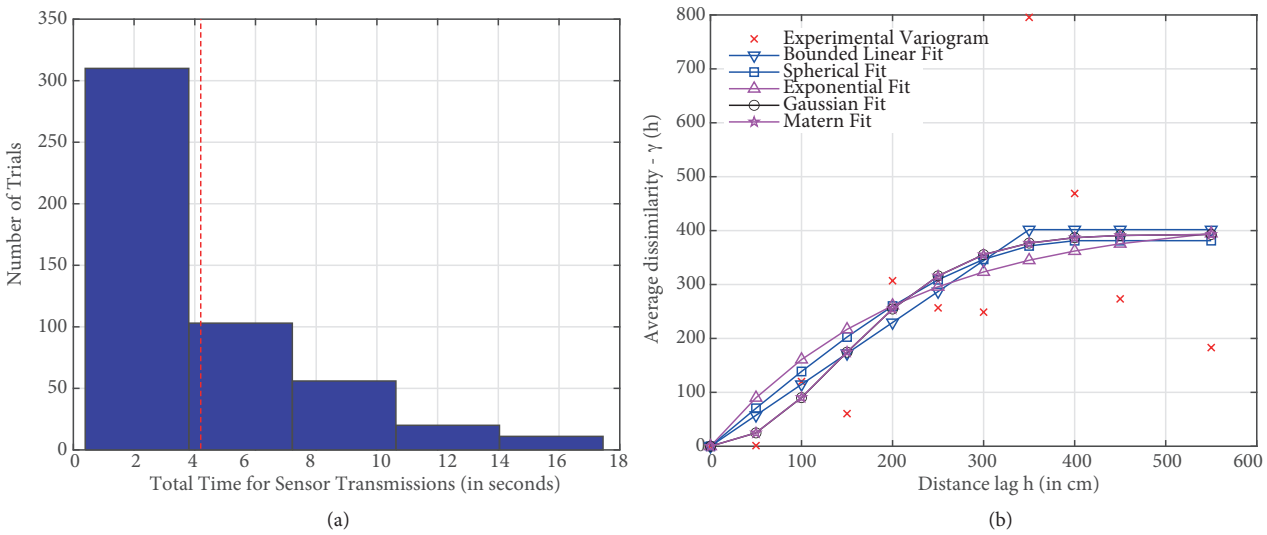

Figure 5. (a) Total transmission time of sensor measurements, (b) experimental variogram and the fitted variogram models.

the field, their close proximity is covered by many other sensors. Therefore, there is strong dependence between the measurement of interest at a given location and the sensor measurements in its vicinity. Due to the success of model fitting in shorter distances as in Figure 5b, we are able to estimate sensor measurements that are close to their actual readings. The test results in Table 3 show that when used with the Gaussian and Matérn variogram models, the relative error between the estimated field and the actual field measurements is less than in the bounded linear, spherical, and exponential models. The Gaussian and Matérn models can model the field with smaller errors. On the other hand, due to its increased number of optimization variables, optimization with respect to the Matérn model may take longer as compared to optimization with respect to the Gaussian model. As an example, for the Gaussian and Matérn models, fmicon determines the optimal values of the variogram parameters in 0.3120 and 0.5160 s, respectively.

Furthermore, in Figure 6, we predict the field intensity over the entire field of interest given in Figure 4a using the measurements of all $N = 11$ sensors. The two neighboring pixels in Figure 6 represent a separation of 3 cm in the field. From Table 3, we choose two variogram models where bounded linear represents a variogram model with relatively large estimation error and Gaussian represents a variogram model with relatively less estimation error. In Figures 6a and 6b, we compute (8) at each pixel to determine the field intensity using bounded linear and Gaussian variogram models, respectively. Then in Figures 6c and 6d we show the estimation error variance at each pixel based on (10). In Figures 6a and 6b, the predicted field intensity over the entire field looks similar in both the bounded linear and Gaussian variogram models. On the other hand, the difference between the two models becomes significant in terms of field estimation variance. The field estimation variance and hence the uncertainty becomes relatively low around the sensor locations and increases towards the bottom regions of the field where there are no sensors. For the inner field, the Gaussian variogram model yields less estimation error variance, and hence less uncertainty, than the bounded linear variogram model. Hence, the Gaussian variogram model results in more accurate estimates rather than the bounded linear, spherical, and exponential variogram models as previously demonstrated in Table 3.

Table 3. Optimized variogram parameters and estimated and actual measurements of the test sensors.

Variogram	Parameter	S_5	S_{10}	S_{11}
Bounded linear	a	350.00	350.00	350.00
	b	414.21	467.57	361.85
	Estimated measurement	83.07	74.02	87.12
	Relative error	0.07	0.11	0.12
Spherical	a	348.03	379.38	432.87
	b	392.16	442.22	351.66
	Estimated measurement	82.44	73.52	88.37
	Relative error	0.06	0.11	0.11
Exponential	a	175.92	139.35	252.95
	b	418.88	447.22	417.14
	Estimated measurement	83.54	74.97	87.30
	Relative error	0.08	0.13	0.12
Gaussian	a	176.38	176.80	220.56
	b	395.78	443.97	369.02
	Estimated measurement	78.63	70.55	97.09
	Relative error	0.02	0.06	0.02
Matérn	a	7.18	7.19	8.99
	b	395.80	443.91	369.27
	v	151.14	151.14	151.14
	Estimated measurement	78.71	70.57	97.04
	Relative error	0.02	0.06	0.02
Actual sensor measurement		77.42	66.42	98.92

6. Conclusions and future work

In this paper, we developed sensors with low power consumption and low cost components, MSP430G2553 as the MCU, nRF24L01+ as the transceiver unit, and LDR as the sensing unit. Using such custom-designed sensors, we formed a proof-of-concept WSN and defined a new addressing scheme to connect 11 sensors to a central fusion center. The sensor measurements were finally used in a field estimation task. In future work, we plan to develop sensors having additional sensing modalities such as temperature, humidity, and pressure. In order to reduce the collisions due to transmissions, rather than requesting measurements from all sensors in the WSN, the variogram model can be first captured from a subset of sensors and then the sensors near the interested location can transmit their measurements. In the proposed sensor design, most of the energy was spent at the communication unit, nRF24L01+, where the communication unit was always on. For energy savings, each sensor can further turn off its communication module for a specific time after successfully sending its measurement to the FC. Finally, in this work, we performed spatial field estimation in a given region of interest. The field estimation problem can be generalized over time and space where both spatial and temporal characteristics of the field need to be determined based on received sensor measurements. Last but not least, rather than field estimation, other applications of statistical inference such as distributed detection, estimation, localization, and tracking can be realized using the developed WSN.

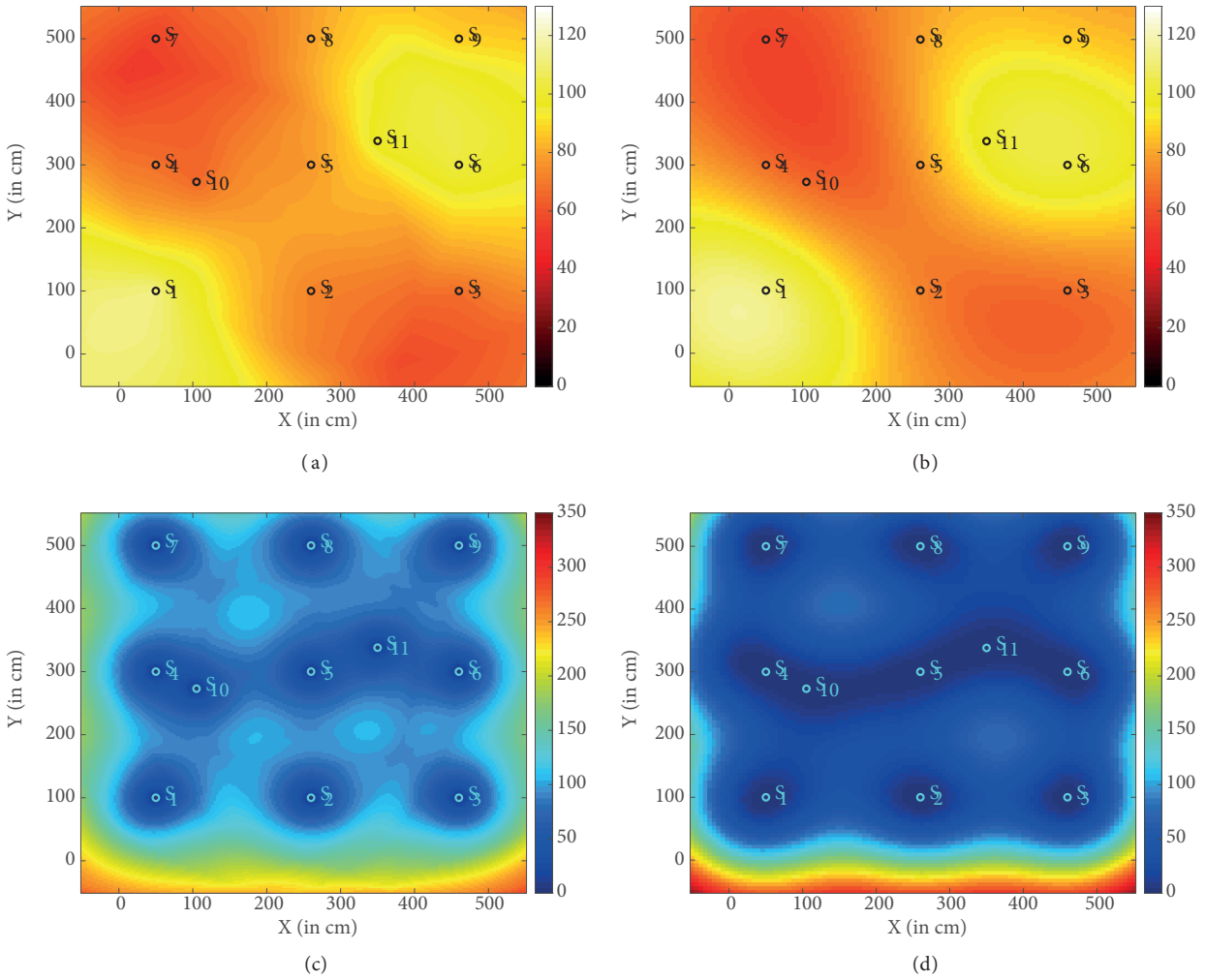

Figure 6. (a) Field reconstruction - bounded linear, (b) field reconstruction - Gaussian, (c) estimation error variance - bounded linear, (d) estimation error variance - Gaussian.

References

[1] Akyildiz IF, Su W, Sankarasubramaniam Y, Cayirci E. A survey on sensor networks. IEEE Communications Magazine. 2002; 40 (8): 102-114, doi: 10.1109/MCOM.2002.1024422

[2] Postigo-Malaga M, Supo-Colquehuanca E, Matta-Hernandez J, Pari L, Mayhua-Lopez E. Vehicle location system and monitoring as a tool for citizen safety using wireless sensor network. In: 2016 IEEE ANDESCON; Arequipa, Peru; 2016. pp. 1–4.

[3] Harrington B, Huang Y, Yang J, Li X. Energy-efficient map interpolation for sensor fields using Kriging. IEEE Transactions on Mobile Computing 2009; 8 (5): 622-635, doi: 10.1109/TMC.2008.167

[4] Jedermann R, Palafox-Albarran J, Barreiro P, Ruiz-Garcia L, Robla JI, Lang W. Interpolation of spatial temperature profiles by sensor networks. In:2011 IEEE SENSORS Proceedings; Limerick, Ireland; 2011. pp. 778-781.

[5] Rahman NAA, Jambek AB. Wireless sensor node design. In: 2016 3rd International Conference on Electronic Design (ICED); Phuket, Thailand; 2016. pp. 332-336.

[6] Uttarkar NK, Kommu A, Kanchi RR. Design and development of data acquisition system for a remote furnace using MSP430G2553 and Zigbee. In: International Conference on Information Communication and Embedded Systems (ICICES2014); Chennai, India; 2014. pp. 1-5.

[7] Ardelean A, Mischie S. Development of an electronic game based on Bluetooth communication. In: 2014 11th International Symposium on Electronics and Telecommunications (ISETC); Timisoara, Romania; 2014. pp. 1-4.

[8] Wang Y, Hu C, Feng Z, Ren Y. Wireless transmission module comparison. In: 2014 IEEE International Conference on Information and Automation (ICIA); Hailar, China; 2014. pp. 902–907.

[9] Weder A. An energy model of the ultra-low-power transceiver nRF24L01 for wireless body sensor networks. In: 2010 2nd International Conference on Computational Intelligence, Communication Systems and Networks; Liverpool, United Kingdom; 2010. pp. 118-123.

[10] Zhao D, Peng C. A small low-power reliable communication module in a wireless monitoring system. In: 2007 1st International Conference on Bioinformatics and Biomedical Engineering; Wuhan, China; 2007. pp. 1194–1197.

[11] Zhang P, Sun L, Zhang P, Hou R, Tian G, Liu X. Wireless network design and implementation in smart home. In: 2013 6th International Conference on Intelligent Networks and Intelligent Systems (ICINIS); Shenyang, China; 2013. pp. 167-170.

[12] Chen S, Yuan YJ. Wireless electronic tourist guide system based on microcontroller. In:2011 IEEE International Conference on Signal Processing, Communications and Computing (ICSPCC); Xi'an, China; 2011. pp. 1–4.

[13] Shi S, Lu T, Zhang H, Xu L, Gulliver TA. A design of active RFID tags based on NRF24L01. In: 2013 10th International Computer Conference on Wavelet Active Media Technology and Information Processing (ICCWAMTIP); Chengdu, China; 2013. pp. 210-213.

[14] Ma Z, Pan X. Agricultural environment information collection system based on wireless sensor network. In: 2012 IEEE Global High-Tech Congress on Electronics; Shenzen, China; 2012. pp. 24-28.

[15] Hao S, Zongtao C. Design of the environmental temperature and humidity wireless monitoring system. In: 2015 12th IEEE International Conference on Electronic Measurement Instruments (ICEMI); Qingdao, China; 2015. pp. 1652–1657.

[16] Ni S, Su J, Nie L, Qu S. Design of multi-point wireless temperature measuring system. In: 2012 Proceedings of International Conference on Modelling, Identification and Control; Hong-Kong; 2012. pp. 422-425.

[17] Chen T, Zhao L. The design of the wireless smart subpoena system based on MSP430. In: 2015 8th International Conference on Intelligent Networks and Intelligent Systems (ICINIS); Tianjin, China; 2015. pp. 153-156.

[18] Chen Z, Hu C, Liao J, Liu S. Protocol architecture for wireless body area network based on nRF24L01. In: 2008 IEEE International Conference on Automation and Logistics; Qingdao, China; 2008. pp. 3050-3054.

[19] Christ P, Neuwinger B, Werner F, Ruckert U. Performance analysis of the nRF24L01 ultra-low-power transceiver in a multi-transmitter and multi-receiver scenario. In: 2011 IEEE SENSORS Proceedings; Limerick, Ireland; 2011. pp. 1205-1208.

[20] Cressie N. Statistics for Spatial Data. Hoboken, NJ, USA: John Wiley & Sons, 2015.

[21] Lichtenstern A. Kriging Methods in Spatial Statistics. B.Sc., Technische Universitat Munchen, Munchen, Germany, 2013.

[22] Kang J, Jin R, Li X. Regression Kriging-based upscaling of soil moisture measurements from a wireless sensor network and multi-resource remote sensing information over heterogeneous cropland. IEEE Geoscience and Remote Sensing Letters 2015;12 (1): 92-96, doi: 10.1109/LGRS.2014.2326775

[23] Akgun VY, Masazade E. Realization of field estimation with sensors designed using low power and low-cost components. In: 2017 25th Signal Processing and Communications Applications Conference (SIU); Antalya, Turkey; 2017. pp. 1–4 (in Turkish with an abstract in English).